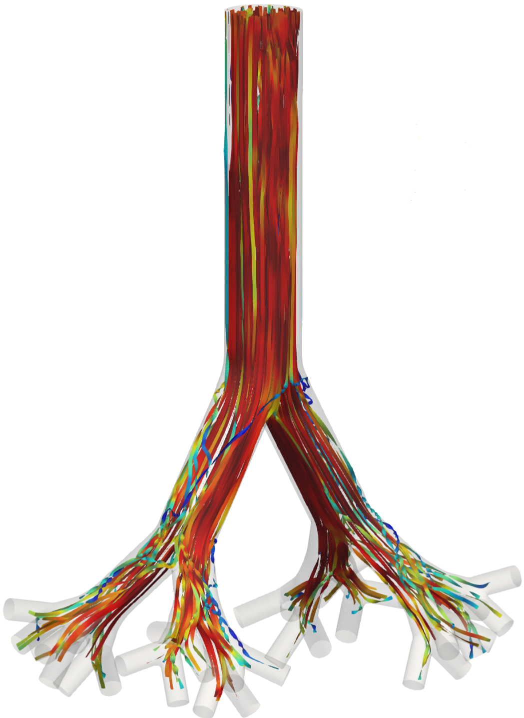

Systematic evaluation of different approaches for modelling inhaled particle deposition in the lung airways

Master's thesis in Applied Mechanics

HARI ABRAM

DEPARTMENT OF MECHANICS AND MARITIME SCIENCES
CHALMERS UNIVERSITY OF TECHNOLOGY
Gothenburg, Sweden 2022
www.chalmers.se

Master's thesis 2022

Systematic evaluation of different approaches for modelling inhaled particle deposition in the lung airways

HARI ABRAM

CHALMERS
UNIVERSITY OF TECHNOLOGY

Department of Mechanics and Maritime Sciences
Division of Fluid Mechanics
Chalmers University of Technology
Gothenburg, Sweden 2022

Systematic evaluation of different approaches for modelling inhaled particle deposition in the lung airways
HARI ABRAM

Supervisor: Erngren Teodor[1], Saeed Salehi[2], Elin Boger[1], Nguyen Duy[1] and Markus Friden[1].
Examiner: Håkan Nilsson[2].

Master's Thesis 2022:29
Department of Mechanics and Maritime Sciences
Division of Fluid Mechanics
Chalmers University of Technology
SE-412 96 Gothenburg
Telephone +46 31 772 1000

Cover: Streamlines of the velocity with a turbulent inlet in the airway geometry.

Typeset in LaTeX
Gothenburg, Sweden 2022

1, AstraZeneca. 2, Chalmers University of Technology

Systematic evaluation of different approaches for modelling
inhaled particle deposition in the lung airways
HARI ABRAM
Department of Mechanics and Maritime Sciences
Chalmers University of Technology

Abstract

A typical path model is an algebraic model utilized to predict the particle deposition in the lung airway geometry. Prediction of particle deposition is an essential part of the drug discovery and manufacturing process. The accuracy of the typical path algebraic model is to be verified and quantified to establish the model's use in future applications.

There exists a variety of typical path models from various authors for particle deposition, this project starts with the comparison of deposition of particles between individual authors and justifies the differences observed between different authors based on the assumptions from which these models are derived. Subsequently, lung CAD geometry is created based on the Yeh and Schum lung dimensions, to properly capture the topology of the lung bifurcations an engineering decision is made to adjust the branching of parent branch into daughter branches.

CFD simulations are performed on the CAD model with the open-source software OpenFOAM. With an inlet flow rate of 60 l/min, the particles are injected into the air, to observe their position of deposition and compare the results of CFD with the typical path model. Deposition efficiency observed for these methods is analyzed and similar and dissimilar general trends are justified. To properly capture the regional deposition the first generation of the lung morphology is divided into different parts, and deposition efficiency in each branch is presented, furthermore observed trends are introduced contrasting the typical path model's broad assumptions.

Keywords: Typical path model, CFD, lung geometry, deposition efficiency, bifurcations, OpenFOAM.

Acknowledgements

First of all, I would like to thank AstraZeneca for giving me an opportunity and resources for this project. This project helped me gain valuable experience that will be instrumental in my future.

I would also like to thank all the people that helped me complete this ardent task in the time allotted for the same. With gratitude to my supervisors, Elin Boger, Erngren Teodor, Nguyen Duy and Markus Friden from AstraZeneca for their support and encouragement throughout the project, along with my supervisor and examiner from the Chalmers University of Technology, Saeed Salehi and Håkan Nilsson for their constructive criticism and valuable feedback. I would like to extend my gratitude to the Annual Review of Fluids for giving me permission to utilize the figure of lung morphology in my report.

Hari Abram, Gothenburg, June 2022

List of Acronyms

Below is the list of acronyms that have been used throughout this thesis listed in alphabetical order:

CAD	Computer-Aided Design
CFD	Computational Fluid Dynamics
DE	Deposition Efficiency
DF	Deposition Fraction
TPM	Typical Path Model

Nomenclature

Below is the nomenclature of indices, parameters, and variables that have been used throughout this thesis.

Indices

i,j	Generation number
t	Index for time step

Parameters

Δt	Time discretization step (time interval)

Variables

$\bar{v}$	Mean velocity
St	Stokes Number
Re	Reynolds Number
P_I	Probability of Deposition due to Impaction
P_S	Probability of Deposition due to Sedimentation
P_D	Probability of Deposition due to Diffusion
D	Diameter of airway
d_p	Diameter of particle
L	Length of branch
ϕ	Gravity angle
θ	Branching angle

Contents

List of Figures

List of Tables

1 Introduction

Treating respiratory diseases through inhaled aerosols and particles is a well-established pharmacotherapy. Deposition of a well-designed inhaled drug at the target site of the disease might lead to a high local exposure while minimizing the systemic exposure and thus the risk of systemic side effects. Clearly, the desired deposition pattern of a drug will depend on the spatial distribution of the pharmacological target and it is thus critical to be able to predict where inhaled particles are deposited.

The procedure to treat respiratory diseases via inhalation was developed rapidly in the early-to-mid 20th century due to the raise in innovative manufacturing processes of plastic nebulizers. With the introduction of the Montreal Protocol in 1987 led to an increase in innovation and transformation that evolved into the diversification of inhaler technologies with significantly enhanced delivery efficiency, including modern MDIs(Metered Dose Inhaler), dry powder inhalers, and nebulizer systems [2]. Modern drug delivery systems depend on deposition modelling to predict the drug deposition in the lung airways, as such, deposition modelling can play a critical role in selecting a particle size distribution, inhalation manoeuvre and/or device that enables deposition in relevant regions. Furthermore, it can also be used to estimate the lung deposited dose and aid in the interpretation of studies.

Currently, the use of in situ experiments to determine the particle deposition in the lungs is limited to a total deposition without spatial resolution. Although, health risk assessment and aerosol therapy require local deposition patterns within the lung airways. Furthermore, experimental data refers to specific human and animal subjects, which cannot be generalized due to the difference in lung and breathing parameters in the general population [19]. Consequently, particle deposition modelling is unavoidable during the design of inhaled aerosols.

The current state of art for the prediction of deposition of the drug relies on two main methods which are listed below:

- Algebraic models based on experimental data. These models depend on the lung and breathing parameters.
- Computational fluid dynamics (CFD) simulations of the inhaled drugs in the lung airway morphology.

There are many advantages to using the algebraic models as a tool for predicting drug deposition, such as low computational cost, ease of use and reasonable accuracy of the results. However, there are also a few disadvantages, such as non-factual assumptions. There are many different algebraic models, one that is straightforward to implement is called the typical path model. The main assumption of the typical path algebraic model is symmetric branching of the tracheobronchial airways, which simplifies the model. This model predicts the deposition of the inhaled drug in each generation of the airway geometry. Here generation corresponds to all the daughter branches of the airway geometry after bifurcation from the parent branch, which is visualized in Figure 2.1.

The use of CFD simulations to predict drug deposition has a higher accuracy since the physics is modelled at higher fidelity. However, the computational resources required for such simulations are prohibitive. So there is a need to combine the higher accuracy of the CFD simulations with the fewer resources and shorter time required by the algebraic models.

Comparison between the deposition prediction by the algebraic model and through CFD is of great interest. Since the algebraic models usually predict the deposition in a generation with the simplified assumptions regarding the influence of the bifurcations and local airway morphology, whereas the CFD forecasts particle deposition based on the fluid transport partial differential equations. Local deposition in a single generation due to the influence of the branching and the three-dimensional nature of the lung geometry can be predicted using CFD. This is not possible with the algebraic models as these models predict the deposition in a generation as a whole. Thus, the results from the CFD can be utilized to improve the algebraic models.

In this project, the upper tracheobronchial airways are simulated and the results from the CFD simulations are compared with those from the typical path model. This report is organised as follows: In Chapter2, the theory behind the typical path model and computational fluid dynamics is elucidated in detail. This is followed by the Chapter3, which presents the methodology used in this thesis with particular emphasis on the difference in the implementation of the algebraic model and CFD. Subsequently, in Chapter4 the results are presented with the particular deliberation on the comparison of deposition prediction by the algebraic model and computational fluid dynamics. At last, this report is concluded in Chapter 5, with the final words regarding the efficiency of different methods and the future outlook for this project.

2

Theory

In the present chapter, the theory behind the algebraic typical path model and computational fluid dynamics (CFD) is elucidated. The assumptions behind the derived equations are presented, since it is instrumental to understand the mechanisms underpinning the deposition for a typical path model to subsequently explain any potential differences as compared to the CFD results. To properly follow the theory behind the typical path model, lung morphology is briefly explained for the reader's assistance.

2.1 Lung Morphology

This section describes the lung airway morphology, with the aim that it would be beneficial to the reader unfamiliar with the lung geometry.

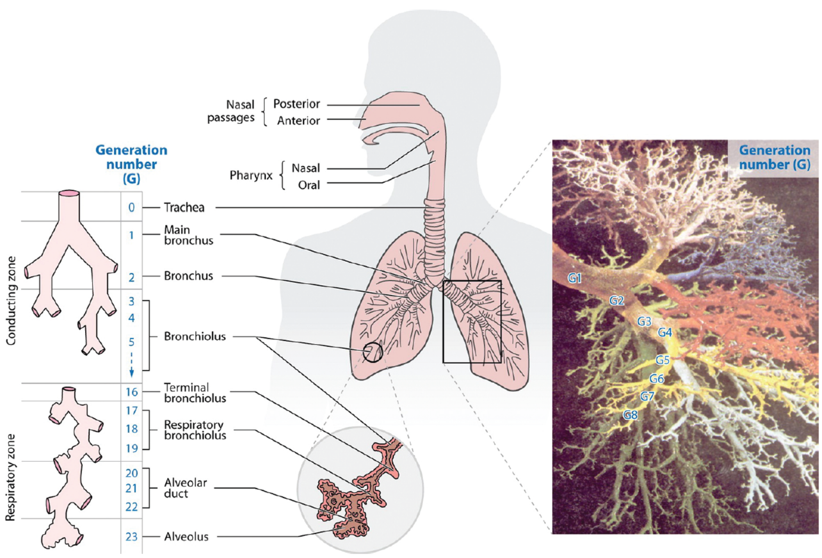

Figure 2.1: Airway morphology (reprinted from [1])

After the inhaled air leaves the upper respiratory system of the nose, nasal cavity and pharynx, it enters the trachea. The trachea bifurcates into a main (or primary) bronchus. These two branches are called the first generation, as mentioned in the introduction. Similarly, all the daughter branches of the main bronchus are called the second generation. The typical path model predicts the deposition generation by generation, rather than regional deposition, as detailed in Section 2.2.

As can be observed from Figure 2.1, the lung morphology is divided into several parts, which can be broadly categorised as follows:

- Trachea, this branch of the lung geometry is called generation 0.
- Conducting zone, which corresponds to generations 1 to 15. This zone comprises bronchi (1-3 generations), bronchioles (4) and terminal bronchioles(5-16)
- Transitional and respiratory zones, composed of respiratory bronchioles (17-19), alveolar Ducts (20 -22) and alveolar Sacs (23).

In this project, the first 6 generations in the tracheobronchial region are considered. Since the comparison between the typical path model and CFD will contribute favourably to the refinement of the typical path model in the first few generations.

2.2 Typical Path Model

The typical path model is an algebraic model implemented to predict the particle deposition in the simplified lung airway morphology. This model is based on the geometry of the Weibel model for the lung, in which it is assumed that there is a symmetric bifurcation of the lung airway at each fork, and all the branches in a single generation are identical, which is visualized in Figure 2.2. As presented in Figure 2.2, after a certain generation the branches are intersecting each other, this is not considered a complication since only a single path from the trachea to alveolar sacs is considered in the typical path model as explained below, and in the CAD model generated for the CFD, this problem is managed as explained in Chapter 3. Weibel A Lung model is a hugely popular simplified lung model that was first introduced by Weibel [3] in 1963, there are many variations based on the Weibel model which are developed for specific cases, eg. Yeh and Schum model [4]. In this project, the model developed by Yeh and Schum is used where the dimensions of the lung airway morphology are developed based on the approximate human lung cast of Rabbe et al. [5].

Since the dimensions of all the branches in a single generation are identical the pathways followed by the inhaled particle from the first generation to the last are also assumed to be identical. Hence, there is a single path from the trachea to alveolar sacs, which corresponds to homogeneous deposition across all the branches in a single generation. The particle or aerosol deposition can be quantified as the Deposition Fraction (DF) or Deposition Efficiency (η or DE) along a particular generation for a typical path model or along a specific region, DF or DE are defined as follows:

$$\mathrm{DF_i} = \frac{\text{Number of particle deposited in a generation i}}{\text{Number of Particles entering the trachea}} \tag{2.1}$$

$$\eta_i \text{ or } \mathrm{DE_i} = \frac{\text{Number of particle deposited in a generation i}}{\text{Number of particles entering generation i}} \tag{2.2}$$

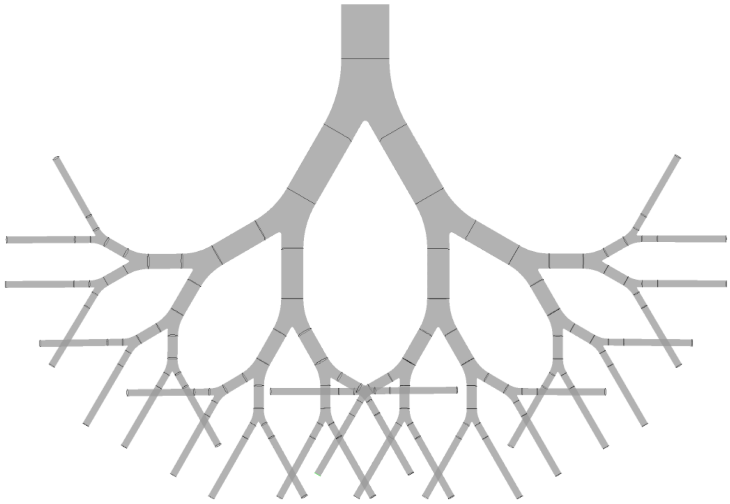

Figure 2.2: Weibel Geometry (reprinted from [6])

Deposition efficiency is identical to the probability of the deposition in a generation due to a particular mechanism.

The tabulated data for the airway geometry [4] for the human lung is presented in Table 2.1.

n	Number of tubes	L (cm)	d (cm)	θ (degrees)	ϕ (degrees)	S (cm^2)	V (cm^3)
0	1	10	2.01	0	0	3.17	31.73
1	2	4.36	1.56	33	20	3.82	16.67
2	4	1.78	1.13	34	31	4.01	7.14
3	8	0.965	0.827	22	43	4.30	4.15
4	16	0.995	0.651	20	39	5.33	5.30
5	32	1.01	0.574	18	39	8.28	8.36
6	64	0.890	0.435	19	40	9.51	8.47
7	128	0.962	0.373	22	36	13.99	13.46
8	256	0.867	0.322	28	39	20.85	18.07
9	512	0.667	0.257	22	45	26.56	17.72
10	1024	0.556	0.198	33	43	31.53	17.53
11	2048	0.446	0.156	34	45	39.14	17.46
12	4096	0.359	0.118	37	45	44.79	16.08
13	8192	0.275	0.092	39	60	54.46	14.98
14	16384	0.212	0.073	39	60	68.57	14.54
15	32768	0.168	0.060	51	60	92.65	15.57

Table 2.1: Typical path model human lung geometry [4]

In Table 2.1, n corresponds to the generation number, L is the length of each tube in the generation, d is the diameter of the tube, θ corresponds to the branching angle, ϕ corresponds to the gravity angle of the tube, S corresponds to a cross-section area of the branch and V corresponds to the volume of a generation. The deposition of the inhaled particle is determined by the various physical mechanisms, which are detailed below.

2.2.1 Deposition mechanisms

As the particle or aerosol travels along the streamlines through the lung airway morphology it experiences different physical mechanisms that result in the particle deposition in the lungs. The typical path models account for the following three different mechanisms: Brownian diffusion, sedimentation due to gravity and impaction due to inertial forces. Different deposition mechanisms play an important role in different regions of lung morphology. Since this project only considers the upper tracheobronchial region, the bulk of deposition in the simulated region will occur as a consequence of impaction due to inertial forces. In the lower tracheobronchial region, the bulk of deposition is due to sedimentation and impaction. In the alveolar region, particle deposition is due to the Brownian diffusion. These mechanisms are visualised in Figure 2.3. The deposition is also influenced by the size and density of the particle, as the larger and higher density particles have higher inertia compared to the smaller particles.

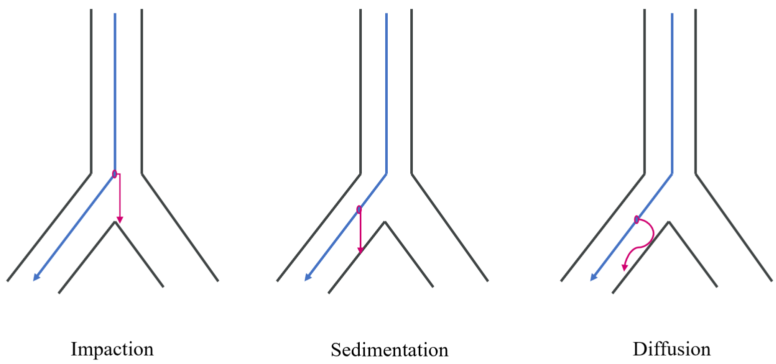

Figure 2.3: Different deposition mechanisms (adapted from [7])

Different deposition mechanisms are explained below in detail.

- Deposition due to impaction occurs when the particle's inertial force is higher than the momentum of the surrounding air precipitating in particle to abandon the air streamlines and get deposited at the lung airway walls.
- Sedimentation of the particles arises in the distal parts of the tracheobronchial region. Since the particle residence time is longer in these regions due to the lower velocity of the air. The particles with larger mass tend to get deposited due to the effect of gravity.

- Diffusion of particles according to the typical path model is due to Brownian motion. Brownian motion can be defined as the random motion of the particles suspended in a medium, this mechanism has a profound effect on particles in the alveolar region of the lung morphology. If the particle size is in the range of 1 µm or less, this mechanism will have a prominent effect, this is due to the interaction of the particle with the air molecules, whose random movement causes the particle to move unpredictably and deposit in lung airways.

2.2.2 Deposition Equations

The equations governing the deposition of the inhaled particles and aerosols for the typical path model are detailed in this subsection. As the typical path model is based on a simplified lung airway geometry, different authors derive and employ distinct equations for the deposition modelling based on the subjects considered. Some of the commonly used equations from different authors for each mechanism are presented below.

2.2.2.1 Impaction

Deposition due to impaction depends on a few main parameters such as Stokes number (St or Stk)[4] and Reynolds number (Re)[4], these are given as:

$$Re = \frac{\rho_f D \bar{v}}{\mu} \tag{2.3}$$

where, ρ_f is the density of the air, D is the diameter of the airway branch, $\bar{v}$ is the mean velocity of the carrier phase and μ is the dynamic viscosity of air.

$$St = \frac{C \rho_p d_p^2 \bar{v}}{18 \mu R} \tag{2.4}$$

where C is the Cunningham slip factor [8], ρ_p is the density of the particle, d_p is the diameter of the particle and R corresponds to the radius of the airway branch. The Cunningham slip factor is defined as :

$$C = 1 + \frac{\lambda}{d_p}\left[2.514 + 0.8\exp\left(-0.55\frac{d_p}{\lambda}\right)\right] \tag{2.5}$$

where λ is the mean free path of the air molecule at room temperature.

The probability of deposition due to impaction as derived by Yeh et al.[4] is given by:

$$P_I = 1 - \frac{2}{\pi}\cos^{-1}(\theta \cdot St) + \frac{1}{\pi}\sin(2\cos^{-1}(\theta \cdot St)) \text{ for } \theta \cdot St < 1 \tag{2.6}$$

$$P_I = 1 \text{ for } \theta \cdot St > 1 \tag{2.7}$$

where,

$$P_I = \text{Probability of deposition due to impaction}$$
$$\theta = \text{branching angle (in radians)}$$
$$St = \text{Stokes number}$$

Lee[8] and Schmid[10] utilize the impaction model developed by the Zhang[9] using dimensional analysis and data fitting of the data obtained from the high fidelity CFD simulations, these equations are given by:

$$P_I = 0.000654 \exp(55.7Stk^{0.954})Re^{(1/3)} \sin(\theta) \text{ for } Stk < 0.04 \tag{2.8}$$
$$= [0.19 - 0.193 \exp(-9.5Stk^{1.565})]Re^{(1/3)} \sin(\theta) \text{ otherwise} \tag{2.9}$$

Yu and Diu [11] developed an impaction deposition model in which they treat airways as a one-dimensional distributed system, this is presented below:

$$P_I = 0.768\beta St \tag{2.10}$$

$$\beta = \frac{L}{4D} \tag{2.11}$$

where L is the length of the branch, D is the diameter of the branch, St is the Stokes number and β is called the bending angle.

Following Landhal's model, Gerrity[12] detailed the probability of deposition due to impaction as given by:

$$P_I(i) = \frac{150\rho_p d_p^2 v_{i-1}}{R_i + 150\rho_p d_p^2 v_{i-1}} \tag{2.12}$$

where $P_I(i)$ corresponds to the probability of deposition due to impaction in ith generation.

Cai and Yu [13] modelled the particle deposition due to the inertia of the particles by integrating across the cross-section of the branch. According to this model, the deposition of the particles depends on the velocity profile at the inlet, based on whether the inlet velocity profile is uniform or parabolic. In this project only a uniform inlet velocity profile is considered:

$$P_I = \frac{4\sin\alpha}{\pi(R_d/R_p)} St \tag{2.13}$$

where R_p is the radius of the parent tube and R_d is the radius of the daughter tube. According to Cai and Yu, the model assumes that there is a constant branching angle $\alpha = 35^o$, with ${}^{R_d}/_{R_p} = 0.67$.

Impaction equations (P_I), according to different authors are based on a few important variables. Such as the branching angle, Reynolds number and Stokes number.

Lee et al.[8], Yeh et al.[4] and Cai et al.[13] derive their equations based on the assumption that the branching angle and Stokes number play an important role in predicting the probability of deposition due to impaction. Since the inertia of the particles depends on the Stokes and Reynolds number. Furthermore, impaction is determined by the change in the flow direction due to the branching angle. Gerrity et al[12] assume that the diameter and velocity play a dominant role in the deposition. These assumptions result in the derived equations being remarkably different from each other. Some of the equations presented here are derived theoretically and others are derived from the experimental or simulated data.

2.2.2.2 Sedimentation

As rationalized in Chapter 2, the deposition due to Sedimentation occurs in airway tubes where the residence time of the particle is longer, and the predominant force acting on the particle during sedimentation is gravity.

Lee[8] and Yu[11] based their deposition efficiency by the sedimentation on the calculation by Thomas[14], as given below.

$$P_S = \frac{2}{\pi}[2\epsilon(1-\epsilon^{2/3})^{1/2} - \epsilon^{1/3}(1-\epsilon^{2/3})^{1/2} + \sin^{-1}(\epsilon^{1/3})] \tag{2.14}$$

where,

$$\epsilon = \frac{3v_g t_i \sin\phi}{4D}$$
$$v_g = \frac{\rho_p d_p^2 g C}{18\mu}$$

here v_g corresponds to the gravitational settling velocity, t_i to the mean residence time in the generation i, g to the gravity and ϕ corresponds to the gravity angle, which is the angle of inclination of the branch with the vertical axis.

According to Yeh[4], the probability of deposition due to sedimentation is calculated as follows:

$$P_S = 1 - \exp\left[\frac{-4gC\rho_p r_p^2 t_i \cos\phi}{9\phi\mu R}\right] \tag{2.15}$$

Gerrity[12] modelled the particle deposition due to sedimentation as follows:

$$P_S = 1 - \exp\left[\frac{-0.8gCv_g t_i \cos\phi}{\mu R}\right] \tag{2.16}$$

Thomas[14] theoretically derived the sedimentation equation (2.14) by assuming that the particles are injected into an inclined pipe. In this setup, the gravity angle (angle between gravity and axis of pipe) and residence time of the particle plays an important role in the probability of deposition due to sedimentation. Similarly, Yeh et al.[4] and Gerrity et al.[12] derived their equations based on the experimental data and dimensional analysis.

2.2.2.3 Diffusion

Deposition due to the diffusion of the particles depends on whether the flow of the carrier phase is laminar or turbulent. According to [11], the probability of deposition due to diffusion is calculated as follows:

For Turbulent flow

$$P_D = 4.0\Delta^{1/2}(1 - 0.444\Delta^{1/2} + ...) \tag{2.17}$$

For laminar flow

$$P_D = 1 - 0.819e^{-14.63\Delta} - 0.0976e^{-89.22\Delta} - 0.0325e^{-228\Delta} - 0.0509e^{-125.9\Delta^{2/3}} \tag{2.18}$$

where

$$\Delta = \frac{D_{mol}L}{D^2\mu}$$
$$D_{mol} = \frac{k_B TC}{3\pi\mu d_p}$$

in which

$$D_{mol} = \text{Brownian diffusion coefficient of the particle}$$
$$k_B = \text{Boltzmann constant}$$
$$T = \text{Temperature}$$
$$C = \text{Cunningham slip factor}$$

Diffusion deposition is modelled based on Ingham's model [23]. The deposition modelling due to diffusion is congruent between different authors with a minute changes in the coefficient of the Δ in equation (2.17), for detailed overview reader is referred to [4, 8, 12, 15]. For the region considered in this project, diffusion doesn't play a dominant role in the deposition. This will be presented in Chapter 4

2.2.2.4 Total Deposition

The previous subsections detail the deposition in a generation due to a specific mechanism, such as impaction, sedimentation or diffusion. The probability of total deposition in a generation is calculated as [12]:

$$P(j) = 1 - (1 - P_I(j))(1 - P_S(j))(1 - P_D(j)) \tag{2.19}$$

where j indicates a generation number, $P(j)$ is the probability of deposition of a particle in generation j and $P_I(j)$, $P_S(j)$ and $P_D(j)$ corresponds to probability of deposition due impaction, sedimentation and diffusion, respectively.

Total deposition during an inspiration phase in a specific generation is calculated from the probability as:

$$DEP(j) = f(j)P(j)\sum_{i=j}^{j_{\max}} V(i) \tag{2.20}$$

where,

$$f(j) = \prod_{i=1}^{j-1}(1 - P(i)) \tag{2.21}$$

Here, $DEP(j)$ is the total deposition in generation j, $V(j)$ is the volume of the j^{th} generation and $j_{\max}$ is the last ventilated generation. This method of calculating total deposition is applicable only for inspiration.

2.3 Computational Fluid Dynamics

CFD is a branch under fluid mechanics dedicated to the numerical modelling of fluid flow or heat transfer using discretization of Navier-Stokes equations. These partial differential equations are based on fundamental laws governing the dynamics of the fluid, which help in the qualitative interpretation of fluid flow parameters and specifications.

2.3.1 Governing Equations

By applying the principles of conservation of energy, mass and momentum on an infinitesimal fluid element present inside a fluid, continuum, momentum and continuity equations are obtained.

The continuity equation is based on the application of mass conservation on the fluid element. The principle of conservation of mass states that the mass of the fluid must remain constant in a fluid element as time advances.

Rate of change of mass in the fluid element	=	Net rate of flow of mass into and out of the fluid element

The differential form of the continuity equation is given as:

$$\frac{\partial \rho}{\partial t} + \frac{\partial(\rho v_i)}{\partial x_i} = 0 \tag{2.22}$$

Where ρ denotes fluid density, t is the time, v_i and x_i is the velocity and the spatial coordinate in the i direction. Since this project concerns the incompressible flow the above equation can be simplified as:

$$\frac{\partial(v_i)}{\partial x_i} = 0 \tag{2.23}$$

which implies divergence of the velocity field is zero.

The momentum equation is also referred to as the Navier Stokes equation and is derived from the application of conservation of momentum on the fluid element. The momentum conservation principle is derived from the Newton's Second Law, which can be stated as,

Rate of change of momentum of the fluid element	=	$\sum$ forces acting on the fluid element

The forces acting on the fluid can be divided into two broad categories. *Surface Forces* (viscous forces and pressure) and *Body Forces* (Gravity).

The momentum equation is given as:

$$\frac{\partial v_i}{\partial t} + \frac{\partial (v_i v_j)}{\partial x_j} = -\frac{1}{\rho}\frac{\partial p}{\partial x_i} + \nu \frac{\partial^2 v_i}{\partial x_j \partial x_j} + \boldsymbol{F} \tag{2.24}$$

Where p is the pressure field, ν is the kinematic viscosity of the fluid and $\boldsymbol{F}$ corresponds to the momentum transfer between injected particles and airflow.

2.3.2 Particle Dynamics

Given an inlet condition where a second phase is injected into the computational domain, there is a need for the coupling between the carrier phase and secondary phase introduced into the air. There are two approaches to the coupling between two phases, these are Lagrangian and Eulerian methods, in this project all the simulations are conducted utilizing Lagrangian methods. The current project implements aerosols as the secondary phase.

In the Lagrangian method, the momentum transfer between the particles and the carrier phase is conducted in two stages. First, the equation of motion for the particle is solved, and then the influence of the particle on the carrier phase is introduced as a force term in Navier-Stokes equations given in (2.24).

The equation of motion for a particle is described by:

$$\frac{d}{dt}(m_p v_i^p) = F_i^D + F_i^L + F_i^{BM} + F_i^G + F_i^{interaction} + ... \tag{2.25}$$

In the Eq (2.25), m_p and v_i^p corresponds to the mass of the particle and velocity vector of the particle, respectively. The forces acting on the particle as it travels through the carrier phase defines and influence the particle trajectory. These forces are F_i^D, F_i^L, F_i^{BM}, F_i^G and $F_i^{interaction}$, which correspond to drag force, lift force, Brownian motion force, gravity force and force of interaction between particles, respectively.

Not all the forces have a comparable influence on the particle trajectory, depending on the event considered and particle aspects that are investigated few of the forces can be neglected. In the present case since the dispersed phase (particulate phase) is dilute particle-particle interactions are neglected. Furthermore, since the carrier air velocity is small the lift force is also neglected. Brownian motion force does not influence the motion of particles at the scales that are considered in this project, since Brownian motion only affects the particles of size 1 microns or less. Whereas the size of particles introduced into the computational domain in this project lies in the range of 2 - 10 microns. The main forces considered for the particle evolution are drag force, gravity and pressure gradient.

Drag force is a force acting on the particle due to the particle geometry, inertia through the carrier phase and relative velocity between the carrier phase and particles. This force is one of the main contributors to the particle equation of motion and is defined as:

$$F_i^D = \frac{1}{2}\rho C_D A_p (v_i - v_i^p)|v_i - v_i^p| \tag{2.26}$$

In Eq.(2.26), ρ is the density of the air, C_D is the drag coefficient of the particle and A_p is the projected particle area. v_i and v_i^p is the velocity of the carrier phase and particles, respectively.

Gravity force is a force acting on the particle due to the gravity, and is defined as:

$$F^G = m_p g(1 - \frac{\rho}{\rho_p}) \tag{2.27}$$

In Eq.(2.27), ρ_p refers to the density of the particles, g refers to the gravitational constant and m_p is mass of the particle.

As the name implies, the pressure gradient force is the force acting on the particle due to the pressure gradient of the carrier phase. This force is dominant in regions with high-pressure gradient, and it is defined as:

$$F_i^{PG} = -V_p \frac{\partial p}{\partial x_i} \tag{2.28}$$

Neglecting diffusive terms and source terms in Eq (2.24), this can be rewritten as the velocity gradient.

$$F_i^{PG} = \frac{m_p}{\rho_p}\rho \left[v_j \frac{v_i}{x_j} + \frac{\partial v_i}{\partial t} \right] \tag{2.29}$$

In Chapter (3), the methods employed in this project are explored in detail, along with the setting and assumptions made for the computational simulations.

3

Methodology

In this chapter implementation of the typical path model and the geometry, mesh and settings used for the CFD simulations are explored in detail. CFD settings for particle dynamics play a vital role in the results obtained, these settings are based on the mesh resolution and turbulence models considered, which will be explored and justified in this chapter. The parameters employed to solve the typical path model equations presented in Chapter 2 are introduced. All the physical parameters used for the typical path model and CFD are equivalent.

3.1 Typical path model

The typical path model equations presented in the Chapter 2 are implemented in the Python programming language. Since these are algebraic equations, the implementation is simple. Airway geometry dimensions utilized in deposition equations are presented in Table 2.1. Table 3.1 presents the constant parameters utilized in solving the deposition equations.

Parameter	Value
Temperature (K)	300
gravity (cm/s^2)	981
ρ_{air}(g/cm^3)	1.225
ρ_{particle}(g/cm^3)	1
Dynamic Viscosity (gm/cm-s)	1.81E-4
Diameter of particle (μm)	10, 5, 2
Boltzmann constant (K_b)	1.3807E-16
Mean free path (nm)	68
Volume flow rate (l/min)	60

Table 3.1: Parameters and their corresponding values

The Python code, in which a typical path model is implemented is presented in Appendix A. As previously explained, the typical path model assumes a single path from the trachea to the last generation. This results in the prediction of deposition efficiency generation by generation. In the code presented, constant and variable physical parameters are utilized along each generation to calculate deposition efficiency for each mechanism. Total deposition in a generation is calculated using deposition efficiency due to different mechanisms, as presented in Eq (2.19). A total deposition is computed for a whole generation, to calculate the deposition in a single branch of a generation, total deposition is divided by the number of branches in a generation. The next section presents the methodology followed to conduct CFD simulations.

3.2 Computational Fluid Dynamics

Open-source software OpenFOAM v2112 is used to conduct the CFD simulations. The simulations performed in this project are Euler-Lagrangian simulations, in which the particles are injected through the inlet and the trajectories of these particles are evolved through time.

3.2.1 Geometry

The lung airway CAD geometry is constructed from the values presented in Table 2.1, main parameters while designing the CAD model is the branching angle and gravity angle, These correspond to the angle made by the daughter branch with the parent branch and with the vertical axis (gravity vector) respectively.

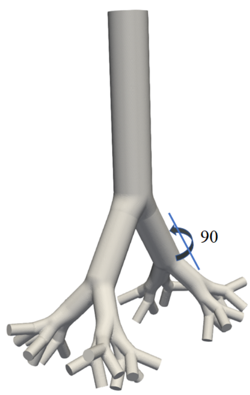

Figure 3.1: Geometry alteration

As previously mentioned, the Weibel A model is a two-dimensional model, which results in the intersection of the branches after a few generations. To overcome this problem in the CAD model the daughter branches are rotated 90 degrees outwards around the axis of the parent branch, as shown in Figure 3.1. The CAD geometry for this project is created in the SpaceClaim software, and the geometry is presented in Figure 3.2. In this figure the first 6 generations of the lung airway morphology are visualized, with separate colours for each generation.

Since parent and daughter branches have different diameters, while designing the CAD model care was taken to ensure that there is a continuous transition from parent to daughter branch. This is achieved as follows, at the outlet of the parent branch two frustums were introduced that will branch into the daughter branch, the larger diameter of the frustum is equal to the diameter of the parent branch and the

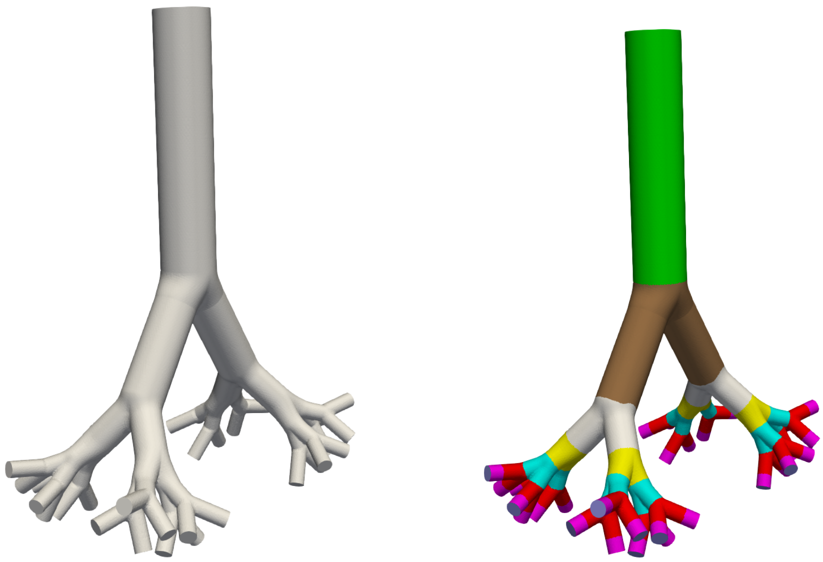

Figure 3.2: Airway geometry with generations coloured

smaller diameter of the frustum is equal to the diameter of daughter branch, these three parts are joined together using a Boolean operation. This method results in a carinal ridge at the bifurcation, Comer et al.[17] have demonstrated that these geometrical adjustments will not affect the flow field in the lung airway geometry.

3.2.2 Solver settings

Transient simulations are conducted in OpenFOAM. The settings for these simulations must correspond to authentic breathing parameters, these settings are controlled through the dictionaries in OpenFOAM software. Some of the important dictionaries and their usage are explained below:

- `controlDict` is used to define the start time, end time and time-step of the simulation. Furthermore, this dictionary can be used to specify the function objects that are needed for the simulation.
- `fvSchemes` is used to designate the time and the space discretization schemes.
- The field residuals and tolerances are specified in `fvSolution` dictionary, along with type a solver for solving the fields.
- `kinematicCloudProperties` is used to evolve the injected particles in lung airway. This dictionary is used to specify the forces acting on the injected particles, along with their density and diameter. This dictionary is also used to specify interactions with each other and boundaries.
- `transportProperties` and `turbulenceProperties` are used to define flow properties and turbulence models used in the simulation, respectively.

The breathing inspiration rate of volume is supposed to be 60 l/min, with aerosols density and diameter as 1 gm/cm^3 and 10 μm, respectively. These parameters are based on the values given in Yeh[4] and Lee[8]. It is assumed that the current simulation is a two-way coupling simulation, this implies that particle-particle interactions are not modelled. Since the volume fraction of the aerosols is negligible compared to the length scale of the computational domain. The number of particles introduced into the computational domain are 100000. The forces acting on the particle are assumed to be a drag, which is modelled using the Ergun, Wen and Yu Drag, gravity and pressure gradient.

`DPMFoam` (Discrete Particle Modeling) Lagrangian solver is used for simulations. In this solver, the continuous phase or fluid phase (air) is solved using the PIMPLE (Pressure Implicit with Splitting of Operators) algorithm and the individual particles are evolved based on the forces acting on a particle as specified.

The total simulation time is 0.5 seconds, with a time step of 5×10^{-6} seconds. A small-time step is essential to make sure that the Courant number is less than 1. `backward` scheme is used for the time discretization, along with the space discretization scheme `linearUpwindV`. All the schemes used are second-order schemes. The residual control for the pressure and velocity is specified as 10^{-4}. The pressure and velocity are under relaxed at the start of the simulation to ensure that pressure and velocity fields converge.

The transport model for the fluid phase (air) is assumed to be Newtonian, with the kinematic viscosity of 1.568×10^{-5} m^2/s, and the density of air is specified as 1.225 kg/m^3. The implicit LES turbulence model (laminar) is used for the simulations, where the subgrid viscosity is assumed to be equivalent to the numerical diffusion present in the simulation.

3.2.3 Mesh

ICEMCFD software is utilized to create the mesh on which CFD simulation is performed. This mesh is converted using an OpenFOAM utility to an OpenFOAM format.

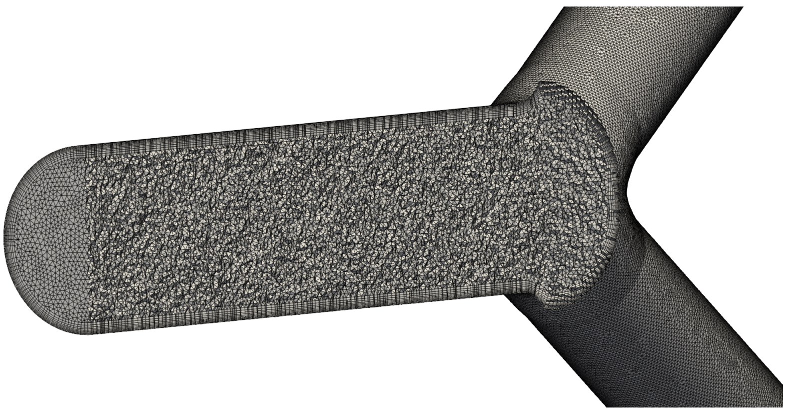

Figure 3.3: Mesh cross-section of the first generation

The mesh created using the airway CAD geometry has six million cells. The justification for the high mesh count for a reasonably simple geometry is that the flow in the computational domain is assumed to be a turbulent flow with the corresponding inlet as a divergence-free turbulent inlet. Hence, to resolve eddies present in the flow necessitates a very fine mesh. This results in a very dense mesh as can be observed in Figure 3.3.

3.2.4 Boundary Conditions

The geometry is divided into 9 boundary patches - Generation 0 - 5, inlet, outlet and auxiliary extrusion near the outlet, this can be visualized in Figure 3.4.

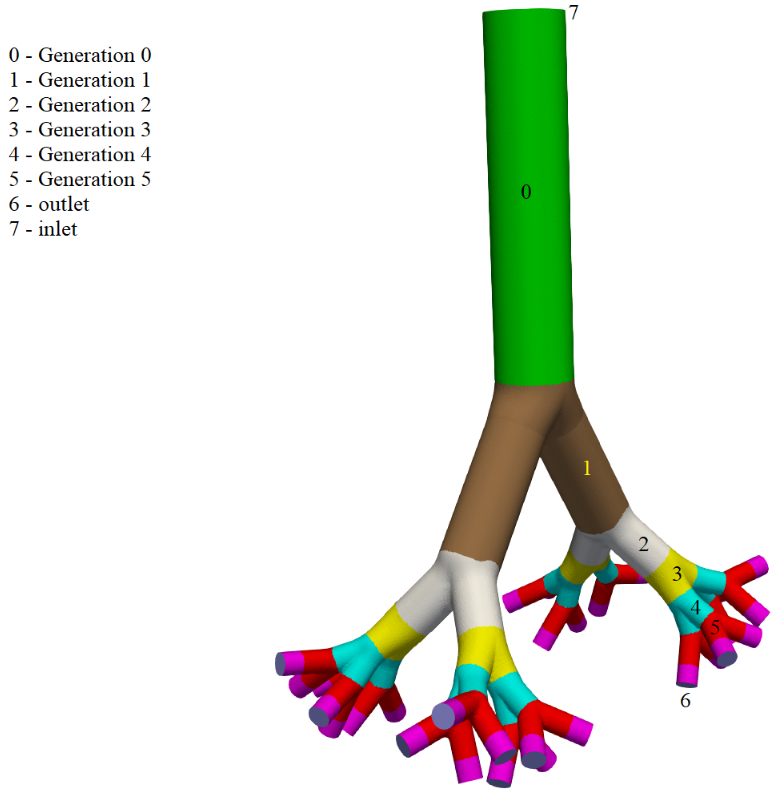

Figure 3.4: Boundaries of the geometry

The walls of the airway geometry CAD model are divided into corresponding generations in such a manner that it would be effortless to differentiate where the particle impinges. The demarcation between daughter and parent branches is assumed at the region where the geometry of the parent branches begins to curve into the daughter branch. Auxiliary extrusion after the 5^{th} generation is because the bifurcation of the 4^{th} generation into 5^{th} generation is in the vicinity of the outlet. This results in the back-flow due to the recirculation generated by the bifurcation, this back-flow results in the divergence of the simulation. To overcome this phenomenon 5^{th} generation is extruded 0.5 cm longer to the outlet. The particles that impinge on this extra wall are removed in post-processing.

In Table 3.2 boundary conditions are presented for pressure and velocity, In the present simulation the inlet is assumed as velocity inlet and the outlet as pressure

Boundary	Patch Type	Boundary Condiition	
		P (pa)	U (m/s)
inlet	velocity inlet	Zero gradient	TurbulentDFSEM inlet
outlet	pressure outlet	0	Zero gradient
Generation 0 - 5	Wall	Zero gradient	No slip
extra wall	Wall	Zero gradient	No slip

Table 3.2: Boundary conditions

outlet, and all the walls are assumed to follow no slip condition. As previously mentioned the inlet velocity is given as turbulent inlet. To specify a turbulent inlet condition OpenFOAM boundary condition `turbulentDFSEMInlet` is utilized, DF-SEM stands for Divergence Free Synthetic Eddy Method. To apply this condition a precursor steady simulation is performed on a cylinder whose dimensions corresponds to the zeroth generation in a lung airway CAD model and with a similar mean velocity profile for a inlet as lung airway. This precursor simulation is performed assuming a periodic boundary condition for inlet and outlet. After the precursor simulation reaches steady state; the velocity, Reynolds stress and integral length scales at the inlet are mapped to the principal simulation.

Mean inlet velocity is calculated assuming a inspiration rate of 60 l/min. An alternative simulation with an uniform constant velocity inlet boundary condition is also performed. The deposition of particles between these two different simulations are compared, along with the typical path model. Furthermore the influence of turbulence on deposition is weighed.

4
Results

This chapter begins with the comparison of deposition efficiency between different typical path models derived by various authors, which are detailed in Chapter 3. Subsequently, the deposition predicted by the CFD simulations for uniform and turbulent inlet is presented. This is contrasted with the typical path model. Furthermore, regional deposition predicted by CFD simulation in first-generation is presented.

4.1 Typical Path Model

As detailed in Section 2.2.2, contrasting equations presented by different authors are implemented in the Python programming language and similitude in the prediction of their deposition efficiency is presented in this section.

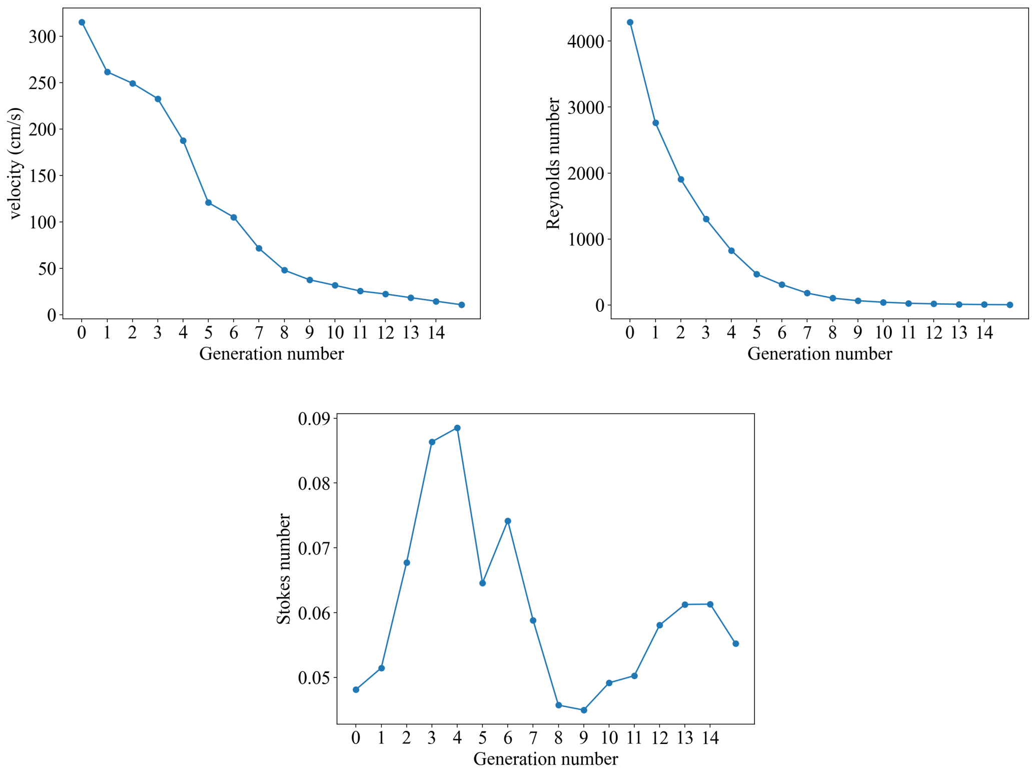

Figure 4.1: Velocity, Reynolds number and Stokes number in each generation

In Figure 4.1, the change in velocity, Reynolds number and Stokes number along with each generation as determined by the typical path model are presented. Velocity and Reynolds number (2.3) are calculated based on the assumption that the flow rate from the parent branch is precisely halved for each daughter branch. This assumption breaks down if compared with the CFD simulation. Stokes number is defined as the ratio of relaxation time of particle with respect to the characteristic time scale of the flow, calculated according to Eq (2.4).

Deposition Efficiency due to different mechanisms and total deposition in each generation according to Lee et al.[8] are plotted in Figure 4.2. The results presented here are for the inhaled particles of size 10µm. Total deposition of the particles predicted by Yeh et al.[4], Yu et al.[11] and Gerrity et al.[12] are presented in Figures 4.3, 4.4 and 4.5 respectively.

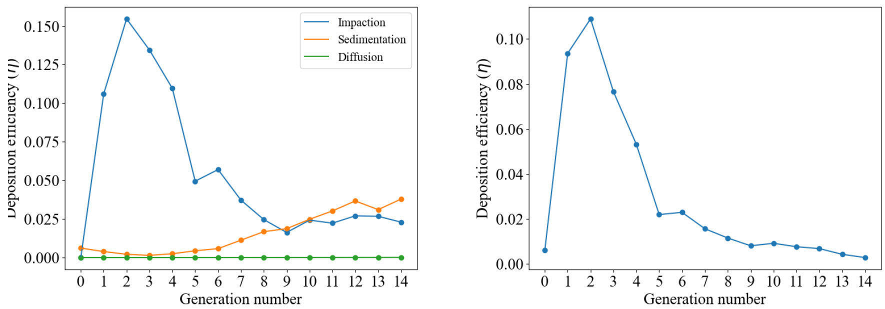

(a) Deposition Efficiency for different mechanism

(b) Total Deposition

Figure 4.2: Deposition prediction according to Lee et al.[8]

As can be observed, total deposition is higher in the generations closer to the inlet with larger diameters. This is caused by the large particle size (10µm) and higher velocities (4.1), this results in the impaction mechanism having a higher influence on the deposition of the particles.

In contrast, it is apparent that in lower bronchial airways sedimentation mechanism has a higher influence on particle deposition due to lower velocities and longer residence time. The influence of diffusion on the particle deposition is negligible for the region of the lung airway considered, as can be observed from the figure.

From Figures 4.2-4.5, it can be observed that the particle deposition is mismatched for different authors. Although depositions prediction by the authors Yeh et al.[4], Yu et al.[11], Gerrity et al.[12] and Cai et al [13] are in the same range compared to Lee et al.[8]. This is due to the method by which the impaction equations are derived by the different authors, Lee et al.[8] utilize the equation obtained by Zhang et al.[9].

In Figure 4.4, showing the deposition prediction based on Yu et al. It can be observed that deposition prediction in the zeroth generation is conflicting when com-

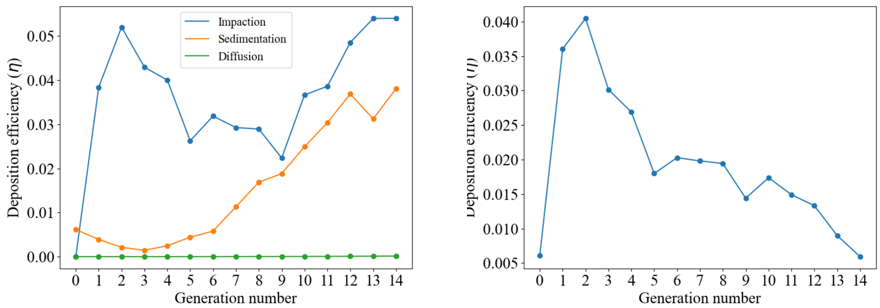

(a) Deposition Efficiency for different mechanism

(b) Total Deposition

Figure 4.3: Deposition prediction according to Yeh et al.[4]

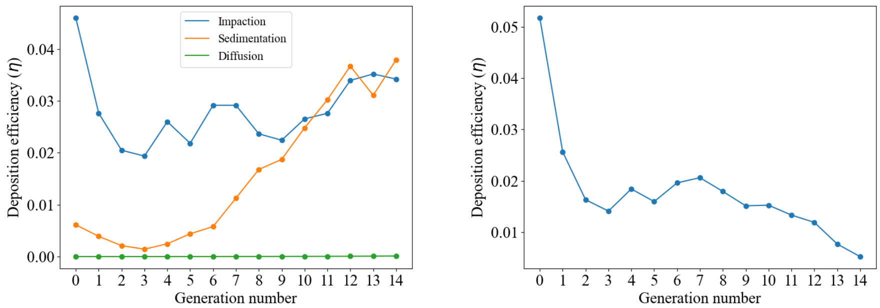

(a) Deposition Efficiency for different mechanism

(b) Total Deposition

Figure 4.4: Deposition prediction according to Yu et al.[11]

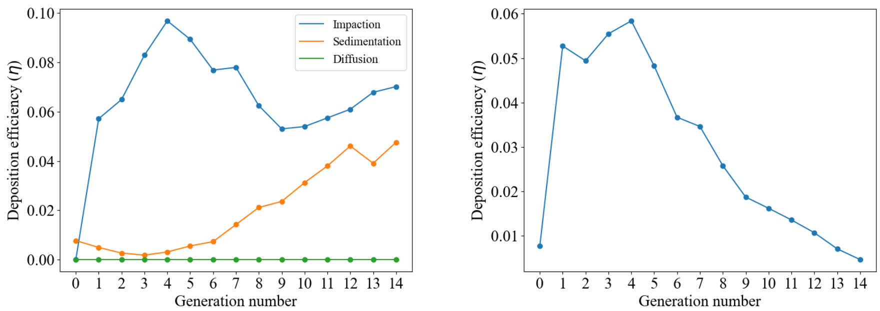

(a) Deposition Efficiency for different mechanism

(b) Total Deposition

Figure 4.5: Deposition prediction according to Gerrity et al.[12]

pared with the other authors. This is due to the method utilized by Yu et al for modelling impaction not availing itself of the branching angle of the bifurcation. Instead, this model utilizes the bending angle which is described by Eq (2.11).

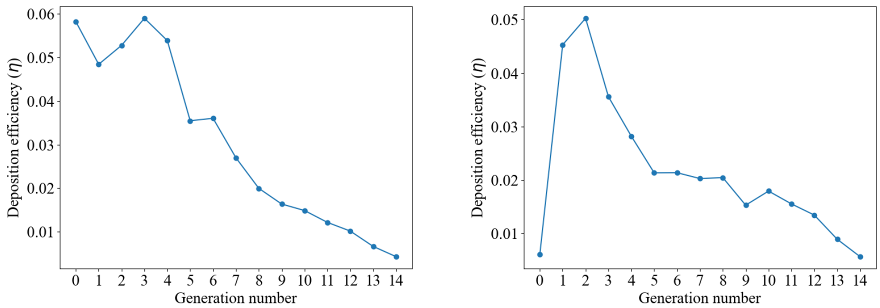

(a) Using the Cai et al dimensions (b) Using the CAD dimensions

Figure 4.6: Total deposition according to Cai et al.[13]

Cai et al.[13] deposition equations are presented in Eq 2.13. This model presents deposition due to impaction mechanisms but the other deposition mechanisms are not derived in [13]. Furthermore, this model is not derived from a specific lung morphology, but by assuming a constant branching angle and an unvarying ratio of daughter and parent branch diameter. The total deposition based on these equations is presented in Figure 4.6. In Figure 4.6(b), the deposition efficiency predicted by Cai et al. based on the lung dimensions of Yeh et al. is presented. It can be observed that the results are notably different compared to Figure 4.6(a), this discrepancy will be discussed in Chapter 5.

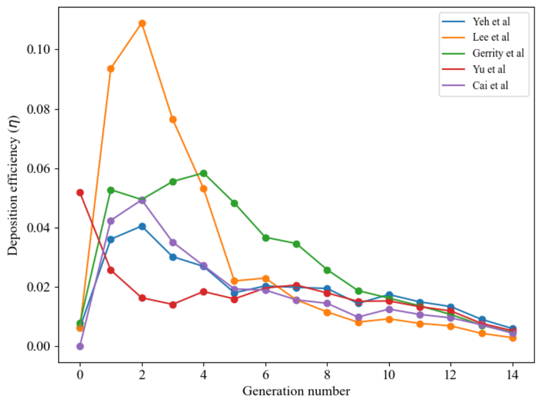

Figure 4.7: Total deposition according to different authors

Figure 4.7 displays the prediction of the deposition according to different authors. It can be observed that there is a wide range of differences between the different authors. To realize among these prediction models which model corresponds to the actual physical process, a comparison with results from CFD is conducted in the next section.

In general, the deposition of the inhaled particles occurs in the first few generations for the particle size considered. In the next section, the deposition of particles calculated by the CFD simulations is presented and compared with the those of typical path model.

4.2 Comparison of CFD and typical path model

Before starting with the comparison of the particle deposition results from the typical path model and the CFD, the comparison is made between a laminar and turbulent inlet velocity boundary condition. To better understand the changes in velocity and pressure for different flow conditions. Furthermore, the similarity between deposition prediction between laminar and turbulent flow is demonstrated.

In Figure 4.8, the contour plot and the streamlines of the velocity for a laminar flow are presented for t = 0.2 s. The contour plot is plotted along the diameter of the zeroth generation. From the figures, it is apparent that there are no velocity fluctuations present in the flow as the streamlines are unswerving. The fluctuations in the velocity are solely due to the geometry of the airway bifurcations. As the flow entering the trachea travels through the nose and pharynx, by the time flow reaches the trachea the velocity profile at the inlet of the trachea is not uniform as assumed here. The particle deposition comparison with the turbulent inlet flow will help in better understanding the significance of laminar and turbulent inlet, which will be presented later.

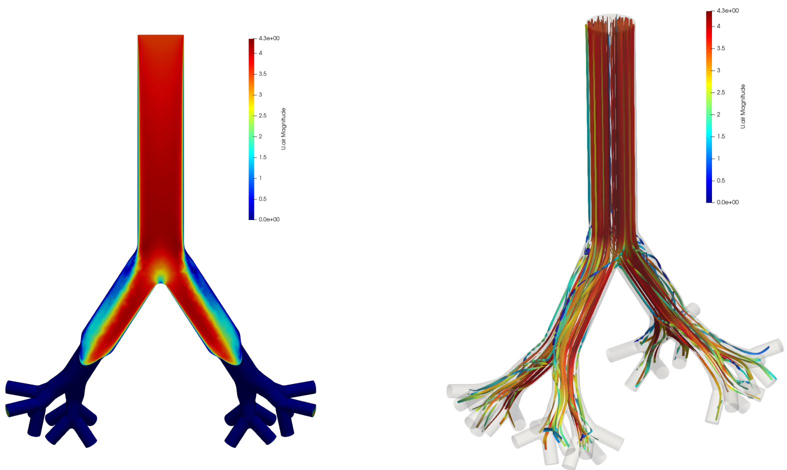

(a) Contour plot of the velocity (U) magnitude

(b) Streamlines of the velocity

Figure 4.8: Laminar flow

Figure 4.9 displays the contour plot and streamlines of the velocity for the turbulent inlet. In this figure, the velocity magnitude is normalized with respect to the maximum laminar velocity for a better comparison.

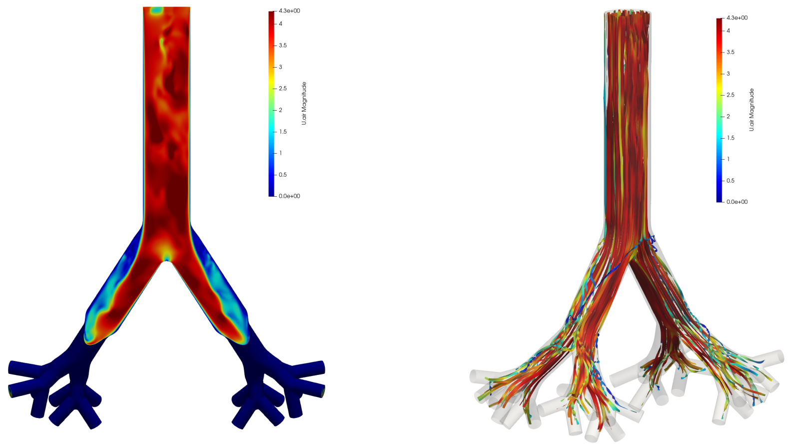

(a) Contour plot of the velocity (U) magnitude

(b) Streamlines of the velocity

Figure 4.9: Turbulent flow

In contrast to the laminar flow presented previously, it can be observed from the velocity contour in Figure 4.9(a) that there are velocity fluctuations present in the zeroth generation. From Figure 4.9(b) it can be observed that the streamlines are not linear, and there is turbulence present in the flow.

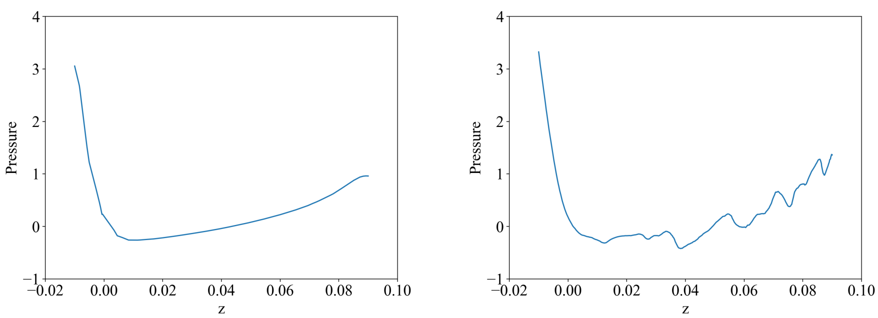

(a) Laminar flow

(b) Turbulent flow

Figure 4.10: Pressure change from inlet to first bifurcation

In Figures 4.10 and 4.11, the change in the pressure and the velocity from the inlet (z = 0.09) to the first bifurcation are presented for laminar and turbulent flow. It can be observed that there is a pressure drop as the air travels through the trachea. In the bifurcation region, there is a sharp increase in pressure due to the stagnation point present in the bifurcation region. From the velocity plot, it can be observed that for turbulent flow there are fluctuations of velocity in span-wise directions, which are not present in laminar flow.

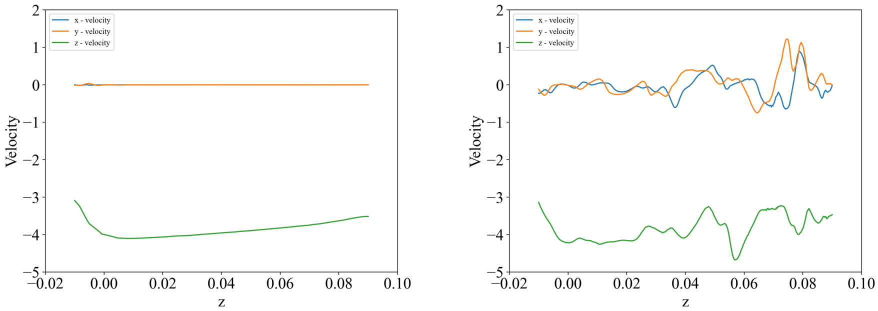

(a) Laminar flow (b) Turbulent flow

Figure 4.11: Velocity from inlet to first bifurcation

Deposition efficiency is calculated as follows for the CFD results:

$$\mathrm{DE_i} \text{ or } \eta_i = \frac{(\text{Number of particles deposited in generation } i)}{\text{Total number of particles injected at the inlet - S(i)}} \tag{4.1}$$

where, S(i) is the sum of the number of particles deposited in generations 0,1...,i-1.

Table 4.1 presents the deposition efficiency calculated by the CFD simulation for the turbulent and laminar flow, this comparison can be visualized in Figure 4.12. From this table, it is evident that the difference in deposition between the two flows is not extreme. Apart from the deposition in the zeroth generation (trachea), where the deposition due to turbulence results in higher deposition compared to laminar flow, as reported by Koullapis et al.[18].

	Total Deposition efficiency in each generation		
Generation number	Uniform (Laminar) inlet (A)	Turbulent inlet (B)	B/A
0	0.00016	0.00078	4.875
1	0.0180329	0.0127099	0.704382
2	0.0353836	0.0273183	0.775763
3	0.0461423	0.0352762	0.7746
4	0.0422308	0.0435661	1.05714
5	0.0931439	0.106247	1.16727

Table 4.1: Comparison of deposition results between the turbulent and uniform (laminar) inlet

This difference in the deposition in the trachea is a consequence of the velocity fluctuations present in the flow due to turbulence. From these results, it can be established that the laminar and the turbulent flow for the geometry considered yield deposition efficiency of the injected particles in the neighbourhood of each other.

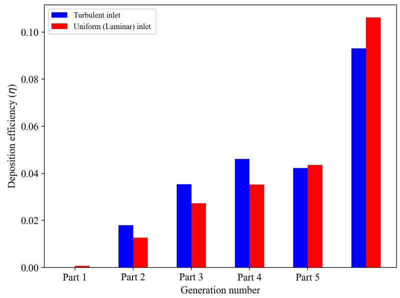

Figure 4.12: Deposition comparison between laminar and turbulent flow

4.2.1 Typical path model

The deposition efficiency of the injected particles according to the typical path model and CFD are compared, and the observed results are justified in this subsection. As previously stated different typical path model equations are compared with CFD results and the model with the least inaccuracy compared to CFD is presented.

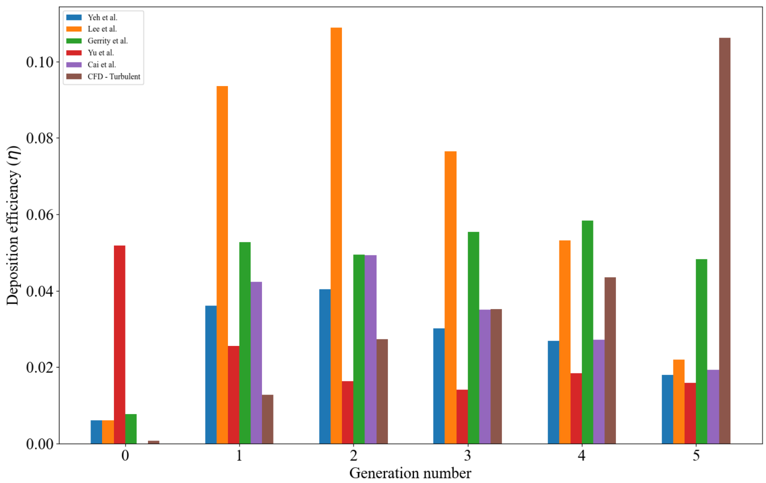

Figure 4.13: Deposition comparison between typical path model and CFD for particles of size 10μm

In Figure 4.13, the comparison of deposition efficiency predicted by CFD and the typical path model are presented. As can be observed from the figure, none of the models are matching precisely with CFD results. This is to be expected since the CFD predicts the deposition by resolving the flow at a higher fidelity compared to the typical path model.

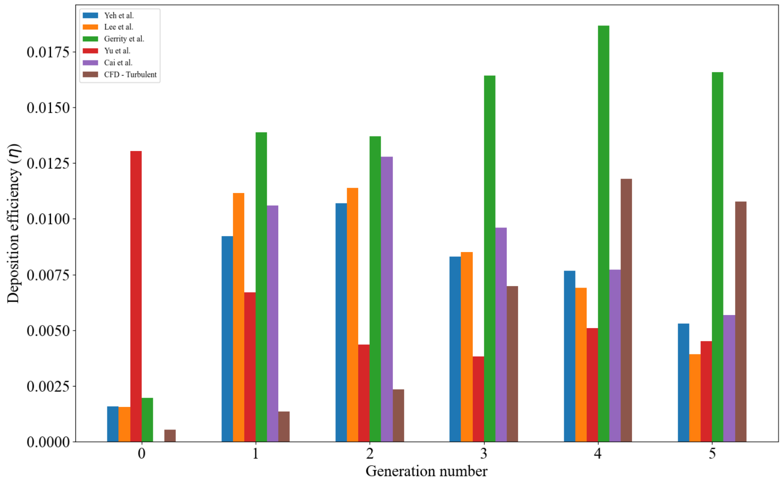

Figure 4.14: Deposition comparison between typical path model and CFD for particles of size 5μm

Figure 4.14 displays comparison of the deposition efficiency for the particles of size 5 microns. It can be observed that the general trend of the deposition is similar to the results presented in Figure 4.13, except for the generations closer to the outlet. Similarly, Figure 4.15 presents results for the particles of size 2 microns.

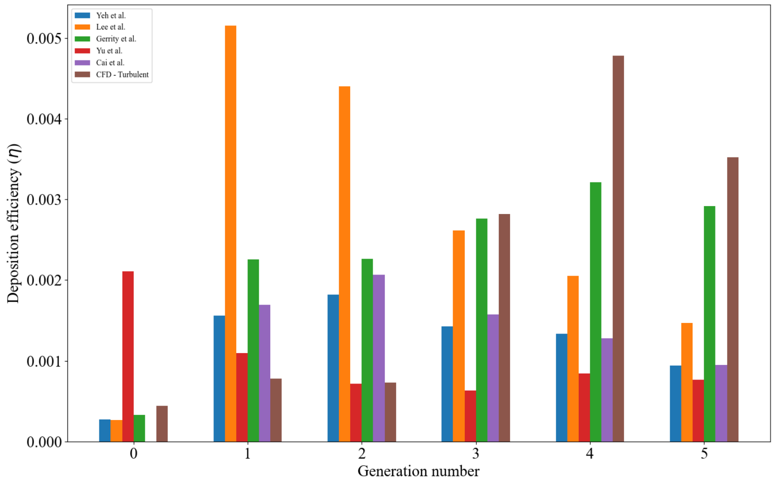

Figure 4.15: Deposition comparison between typical path model and CFD for particles of size 2μm

The comparison presented here offers a better understanding of the accuracy of prediction of particle deposition determined by the typical path model as opposed to

CFD. In Figure 4.16 the particles deposited in the lung geometry are visualized, where it can be observed that the deposition predominantly occurs at the bifurcation region.

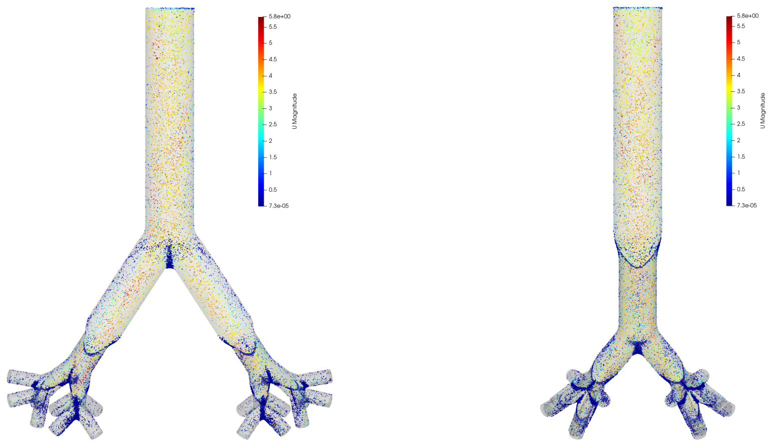

(a) Y-Z plane (b) X-Z plane

Figure 4.16: Particle deposition in the lung geometry

To properly understand the regional deposition in a generation, the first generation is divided into different parts as presented in Figure 4.17. In Figure 4.17(b), the particles that are deposited on the lung walls are enlarged, as opposed to the particles that are still active (or transported by the air).

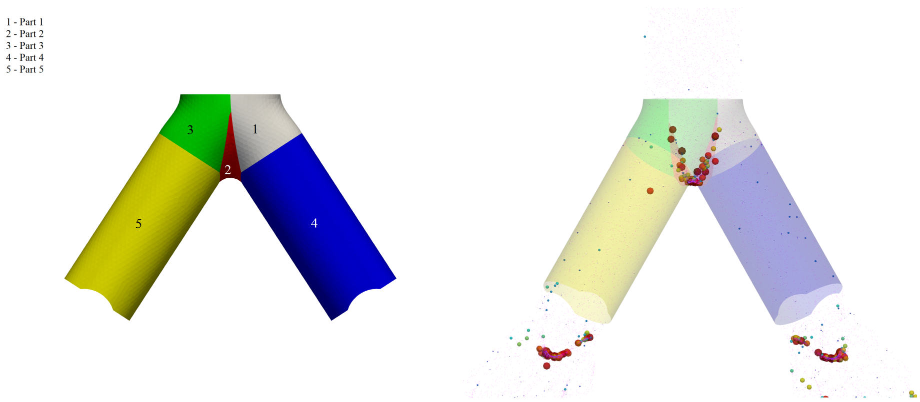

(a) Geometry boundaries (b) Particle deposition

Figure 4.17: Particle deposition in different parts of Generation 1

The deposition of the particles in each part of generation is presented in Figure 4.18. It is observed that highest deposition occurs in the bifurcation region. This is unavoidable as the particles inertia transports the particles parallel to the axis of previous generation resulting in particles depositing in the bifurcation region.

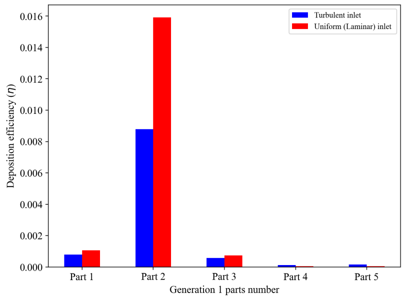

Figure 4.18: Regional deposition

According to the figure there is significant difference in the deposition of the particles between the turbulent and laminar flows. This is due to velocity fluctuations present in the flows that influences the particle trajectories. It can be noted that the particle deposition in the two daughter branches is dissimilar.

From the results presented previously it can be concluded that particle deposition prediction by different methods have a high variance among each other. These differences are due to various reasons such as assumptions made while deriving the typical path model equations, and the CAD geometry constructed for the CFD simulations. Notwithstanding the variance in the prediction results from the different methods the results obtained are in same range. From which it can be deduced that the deposition mechanisms and the physics behind the typical path model and CFD are similar.

5

Discussion and Conclusion

The need for satisfactory methods to predict the inhaled particle deposition in the lung morphology is expanding due to the increased accuracy required for modern pharmacotherapy and raising air pollution across the world. Present methods that are used ubiquitously such as the typical path model need to be improved. This project aims to detect the algebraic typical path models that are proportionate to the results obtained using CFD. Furthermore, regional deposition across the generation is calculated using CFD simulations.

In Chapter 4, high variance is observed between the results obtained from different models. For example, Yu et al.[11] predict higher deposition in zeroth generation (trachea) compared to other authors, but from CFD results it is apparent that in trachea there will be smaller deposition compared with other generations. This is due to the fact that Yu et al.[11] assume that the deposition as a consequence of impaction is predominantly due to the diameter and length of the branch. Cai et al.[13] derived their model based on simplified dimensions and assumptions as explained in Chapter 3. As previously presented, the model developed by Cai et al.[13] applied to Yeh and Schum lung geometry presents results that are similar to the other authors.

Simultaneously, Lee et al.[8] predict a higher deposition of the particles compared to the other authors and CFD in the 1-3 generations. Owing to the fact that for a small Stokes number the deposition is proportional to the Reynolds number of the flow. Considering these observations it is suggested that the models developed by Yeh et al.[4], Gerrity et al.[12] and Cai et al.[13] should be employed for the prediction of particle deposition depending on the particle size. The difference between the deposition efficiency predicted by the typical path model and CFD is smaller for smaller particles.

There is a disagreement between results obtained by CFD and typical path models. As presented previously typical path models predict a higher deposition of particles in generations closer to the inlet and contrastingly lower deposition in 5^{th} generation for larger particles. The CFD results obtained for the geometry considered in this project for 5^{th} generation should be circumspect. Since the outlet of the computational domain is in a neighbourhood of the flow separation region. This results in a recirculation region in the 5^{th} generation, which in turn results in larger residence time for the particles in the generation.

As the flow travels from the parent to the daughter branch it is compressed in one direction and expanded in a perpendicular direction. Due to the differences in the diameter from the parent to daughter branches and the CAD geometry developed in this project. This results in an increase in the fluid (air) velocity at the inlet of the daughter branches. Developing in the particles being pulled along the flow streamlines despite the fact that particle's inertia should be strong enough to escape the flow and deposited in the branches. This could be the reason behind the large discrepancy between the results from typical path models and CFD in the generations closer to the inlet.

The general trend observed in the typical path models with a decreasing deposition efficiency corresponding to an increasing generation number is unobserved in the CFD results. As mentioned previously deposition of particles depends on a broad range of inter-connected mechanisms with dependency on the lung geometry and structure. This may result in different mechanisms influencing deposition in different models. Nevertheless for the region of the lung airway considered in this project the general trend observed in CFD results for particle deposition is similar to CFD results from Zhang et al.[20].

Another observation to be aware of is that the typical path model assumes a constant uniform flow velocity in a generation, which is not observed in CFD simulations. This can be visualized from the contour plots presented in Chapter 4. In this regard the particles have different velocities in a single branch of a generation, resulting in different mechanisms influencing a deposition in generations closer to the inlet. As opposed to the typical path model, in which deposition depends on the constant fluid (air) velocity in a branch. Resulting in the prediction that closer to inlet probability of deposition due to inertia is higher compared to other mechanisms, contrary to the results from the CFD simulation.

Previously the comparison of deposition along a generation for different methods is presented and discussed. This does not suggest the regional deposition or spatial distribution of the particle deposition in a generation. To tackle this problem the generation is divided into different parts and deposition efficiency obtained from the CFD simulation in each part is analyzed. From the results obtained it is apparent that the deposition occurs predominantly at the bifurcation. This is to be expected as the deposition due to inertia ensues on account of the obstruction in flow. This finding has major implications on predictions of drug concentration at the target site, which will be under-predicted if the initial conditions are provided by a typical path model, which cannot describe these so-called hot spots. As such, combining CFD simulation with physiologically-based models could provide a step-change when it comes to predicting local concentrations following inhalation.

5.1 Future Work

In this project, the lung CAD geometry generated is based on many assumptions. This results in the transport of air through a geometry dissimilar to the actual lung geometry. It could be beneficial in understanding the deposition predicted from generation to generation for the actual lung geometry compared to the Weibel A lung model and recognising contrasting mechanisms underpinning the deposition in different geometries.

Regional deposition in the first generation is presented. From the analysis of these results, it is apparent that deposition predominantly occurs at the bifurcation region of a generation. From these results, the typical path model can be improved to predict regional deposition. Establishing the improved typical path model equations from the CFD results requires huge quantities of data, constructed from different geometries and boundary conditions for the simulations.

Bibliography

[1] Kleinstreuer,C., Zhang,Z: Airflow and particle transport in the human respiratory system.

[2] Stephen W Stein., Charles G Thiel: The History of Therapeutic Aerosols: A Chronological Review

[3] Ewald R Weibel: Morphometry of the Human Lung.

[4] Hsu-Chi Yeh., Schum,G,M: Models of Human Lung Airways and Their Application to Inhaled Particle Deposition.

[5] Raabe,O,G., Yeh,H,C., Schum,G,M., Phalen,R.F: Tracheobronchial Geometry : Human, Dog, Rat, Hamster.

[6] B Schöneberger., M Kölbel., A,Delgado: Numerical study of a 5-generation Weibel lung compared to experiments.

[7] Muchao,F,P., Filho,L,V: Advances in inhalation therapy in pediatrics.

[8] Dong Youb Lee., Anthony S,Wexler: Particle deposition in juvenile rat lungs:A model study.

[9] Zhang,L., Asgharian,B., Anjilvel,S: Inertial deposition of particles in the human upper airway bifurcations.

[10] Otmar Schmid., Ines Bolle., Volker Harder., Erwin Karg., Shinji Takenaka., Holger Schulz., and George A. Ferron: Model for the Deposition of Aerosol Particles in the Respiratory Tract of the Rat. I. Nonhygroscopic Particle Deposition.

[11] Yu,C,P: Exact Analysis of Aerosol Deposition during the steady breathing.

[12] Timothy R Gerrity., Peter S Lee., Frank J Haas., Anthony Marinelli., Peter Werner., Ruy V Lourenco: Calculated deposition of inhaled particles in the airway generations of normal subjects.

[13] F,S,Cai., C,P,Yu: Inertial and Interceptional Deposition of Spherical Particles and Fibers in a Bifurcating Airway.

[14] Jess W. Thomas: Gravity Settling of Particles in a Horizontal Tube.

[15] Cheng,Y,S: Condensation detection and diffusion size separation techniques.

[16] Natalya Nowak., Prashant P Kakade., Ananth V Annapragada Computational Fluid Dynamics Simulation of Airflow and Aerosol Deposition in Lungs.

[17] Comer,J,K., C Kleinstreuer., Z Zhang: Flow structures and particle deposition patterns in double-bifurcation airway models. Part 1. Air flow fields.

[18] P,G,Koullapis., L,Nicolaou., S,C,Kassinos: *In silico* assessment of mouth-throat effects on regional deposition in the upper tracheobronchial airways.

[19] Werner Hofmann: Modelling inhaled particle Deposition in the human lung - A Review.

[20] Zhang,Z., Kleinstreuer,C., Kim,C,S: Comparison of analytical and CFD models with regard to micron particle deposition in a human 16-generation tracheobronchial airway model.

[21] Vaish Mayank: Lung-Aerosol Dynamics in Human Airway Models: Validation and Application of OpenFOAM Software.

[22] Yun Hwan Kim: CFD modelling of air flow and fine powder deposition in the respiratory tract.

[23] Ingham,D,B: Diffusion of aerosols from a stream flowing through a cylindrical tube.

A

TPM Python code

```python
import os
import sys
import numpy as np
import matplotlib.pyplot as plt
import scipy as sp

class typical_path_model():

    def __init__(self,data,D_particle,author='Lee'):
        self.data = data
        self.K_b =  1.3807E-16
        self.Temp = 300
        self.g = 9.81E2 #cm/s2
        self.rho_fluid = 1.225E-3 #g/cm3
        self.rho_particle = 1 #g/cm3
        self.dyna_visc = 1.81E-4 #g/cm-s
        self.D_particle = D_particle #cm
        self.MFP = 68E-9 * 1E2 #cm
        self.L = data[:,1] #cm
        self.D = data[:,2]
        self.theta = data[:,3]
        self.phi = data[:,4]
        self.VFR = data[:,8]
        self.author = author

        self.m = len(data[:,0])
        self.u_fluid = np.zeros((self.m,))
        U_fluid_i = data[0,8]/(np.pi*(self.D[0]**2)/4)
        self.u_fluid[0] = U_fluid_i

        for i in range(1,self.m):
            self.u_fluid[i] = data[0,8]/((2**i)*(np.pi*(self
              .D[i]**2)/4))


        self.Stk = (self.rho_particle*(self.D_particle**2)*
```

```
        self.u_fluid)/(18*self.dyna_visc*self.D)
    self.Re = (self.rho_fluid*self.D*self.u_fluid)/(self
        .dyna_visc)

    self.t_i = self.L/self.u_fluid

    self.DF_i = np.zeros((self.m,)) #Deposition
        efficiency due to impaction
    self.DF_d = np.zeros((self.m,)) #Deposition
        efficiency due to diffusion
    self.DF_s = np.zeros((self.m,)) #Deposition
        efficiency due to sedimentation



def Impaction(self):

    if self.author.lower() == 'lee':
        for i in range(self.m):
            if self.Stk[i] < 0.04:
                self.DF_i[i] = (0.000654*np.exp(55.7*(
                    self.Stk[i]**0.954))*(self.Re[i
                    ]**(1/3))*np.sin(self.theta[i]*np.pi
                    /180))
            else:
                self.DF_i[i] = ((0.19-(0.193*np.exp
                    (-9.5*(self.Stk[i]**(1.565)))))*(self
                    .Re[i]**(1/3))*np.sin(self.theta[i]*
                    np.pi/180))

    if self.author.lower() == 'yeh':
        Cun_slip = 1+((2*self.MFP/self.D_particle)
            *(1.257+(0.4*np.exp(-0.55*(self.D_particle/
            self.MFP)))))
        Stks = (Cun_slip*self.rho_particle*(self.
            D_particle**2)*self.u_fluid)/(18*self.
            dyna_visc*self.D)
        for i in range(self.m):
            if self.theta[i]*Stks[i]*np.pi/180 >= 1:
                self.DF_i[i] = 1
            else:
                self.DF_i[i] = 1- ((1/np.pi)*((2*np.
                    arccos(self.theta[i]*Stks[i]*np.pi
                    /180))-np.sin(2*np.arccos(self.theta[
                    i]*Stks[i]*np.pi/180))))
```

```
        if self.author.lower() == 'yu': # no theta
            self.DF_i = 0.768*self.Stk*self.L/(4*self.D)

        if self.author.lower() == 'gerrity':
            s = (150*self.rho_particle*(self.D_particle**2)*
                self.u_fluid[:-1])
            self.DF_i[1:] = (s/
                            ((self.D[1:]*0.5)+s))

        if self.author.lower() == 'cai':
            R = ((self.D[1:]/self.D[:-1]))
            R = R.tolist()
            R.append(R[-1])
            R = np.array(R)
            self.DF_i = self.Stk*4*np.sin(self.theta*np.pi
                /180)/(np.pi*R)


        return self.DF_i



    def Sedimentation(self):

        if self.author.lower() == 'lee' or self.author.lower
            () == 'yu' or self.author.lower() == 'cai':
            Cun_slip = 1+((2*self.MFP/self.D_particle)
                *(1.257+(0.4*np.exp(-0.55*(self.D_particle/
                self.MFP)))))
            self.v_g = (self.rho_particle*(self.D_particle
                **2)*self.g*Cun_slip)/(18*self.dyna_visc)
            self.epsilon = (3*self.v_g*self.t_i*np.cos(self.
                phi*np.pi/180))/(4*self.D)
            self.DF_s = (2/np.pi)*((2*self.epsilon*((1-(self
                .epsilon**(2/3)))**(1/2))) - ((self.epsilon
                **(1/3))*((1-(self.epsilon**(2/3)))**(1/2)))
                + np.arcsin(self.epsilon**(1/3)))

        if self.author.lower() == 'yeh':
            Cun_slip = 1+((self.MFP/self.D_particle)
                *(2.514+(0.8*np.exp(-0.55*(self.D_particle/
                self.MFP)))))
            self.DF_s = 1-np.exp((-4*self.g*Cun_slip*self.
                rho_particle*(self.D_particle**2)*self.L*np.
                cos(self.phi*np.pi/180))/(18*np.pi*self.
                dyna_visc*self.D*self.u_fluid))
```

```
        if self.author.lower() == 'gerrity':
            Cun_slip = 1+((2.63E-6)*(6.23+(2.01*np.exp(-8.32
                E4 * self.D_particle)))/self.D_particle)
            self.v_g = (self.rho_particle*(self.D_particle
                **2)*self.g*Cun_slip)/(18*self.dyna_visc)
            self.DF_s = 1-np.exp(-1.6*self.v_g*self.t_i*np.
                cos(self.phi*np.pi/180)/self.D)

        return self.DF_s

    def Diffusion(self):

        if self.author.lower() == 'lee' or self.author.lower
            () == 'yu' or self.author.lower() == 'cai' :
            Cun_slip = 1+((self.MFP/self.D_particle)
                *(2.514+(0.8*np.exp(-0.55*(self.D_particle/
                self.MFP)))))
            D_mol = (self.K_b*self.Temp*Cun_slip)/(3*np.pi*
                self.dyna_visc*self.D_particle)
            self.Delta = (D_mol*self.L)/(self.u_fluid*(self.
                D**2))

            self.DF_d = (1 - (0.819*np.exp(-14.63*self.Delta
                )) - (0.0976*np.exp(-89.22*self.Delta)) -
                (0.0325*np.exp(-228*self.Delta)) - (0.0509*np
                .exp(-125.9*(self.Delta**(2/3)))))

        if self.author.lower() == 'yeh':
            Cun_slip = 1+((self.MFP/self.D_particle)
                *(2.514+(0.8*np.exp(-0.55*(self.D_particle/
                self.MFP)))))
            D_mol = (self.K_b*self.Temp*Cun_slip)/(3*np.pi*
                self.dyna_visc*self.D_particle)
            self.Delta = (D_mol*self.L)/(self.u_fluid*(self.
                D**2))

            self.DF_d = (1 - (0.819*np.exp(-7.315*self.Delta
                )) - (0.0976*np.exp(-89.22*self.Delta)) -
                (0.0325*np.exp(-228*self.Delta)) - (0.0509*np
                .exp(-158.62*(self.Delta**(2/3)))))

        if self.author.lower() == 'gerrity':
            Cun_slip = 1+((2.63E-6)*(6.23+(2.01*np.exp(-8.32
                E4 * self.D_particle)))/self.D_particle)
            self.DF_d = 1-np.exp(-8E-6*np.sqrt(Cun_slip*self
```

```
                .t_i*self.D_particle)/self.D)

        return self.DF_d

if __name__ == '__main__':
    data = np.loadtxt('airway_geometry_specifications',
        delimiter=',')
    D_particle = 10E-4 # centimeter
    author = 'yu'

    TPM = typical_path_model(data=data,D_particle=D_particle
        ,author = author)
    V_gen = data[:,6]

    DF_i = TPM.Impacation()
    DF_s = TPM.Sedimentation()
    DF_d = TPM.Diffusion()
    np.append(DF_i,[DF_i[-1]])

    Prob = 1 - ((1-DF_i)*(1-DF_s)*(1-DF_d))

    Deposition = np.zeros((len(Prob),))
    Deposition[0] = Prob[0]*sum(V_gen[0:])/sum(V_gen[0:])

    for i in range(1,len(Prob)):
        F = 1
        for j in range(i):
            F = F*(1-Prob[j])
        Deposition[i] = F*Prob[i]*sum(V_gen[i:])/sum(V_gen
            [0:])
```

DEPARTMENT OF MECHANICS AND MARITIME SCIENCES
CHALMERS UNIVERSITY OF TECHNOLOGY
Gothenburg, Sweden
www.chalmers.se

CHALMERS
UNIVERSITY OF TECHNOLOGY